HHS Public Access

Author manuscript

Mucosal Immunol. Author manuscript; available in PMC 2020 June 02.

Published in final edited form as:

Mucosal Immunol. 2020 March ; 13(2): 230–244. doi:10.1038/s41385-019-0237-2.

Adaptation to inflammatory acidity through neutrophil-derived adenosine regulation of SLC26A3

Ian M. Cartwright[1,2,3,*], **Valerie F. Curtis**[1,2,*], **Jordi M. Lanis**[1,2], **Erica E. Alexeev**[1,2], **Nichole Welch**[1,2], **Matthew S. Goldberg**[1,2], **Rachel E.M Schaefer**[1,2], **Rachel Y. Gao**[1,2], **Carlene Chun**[1,2], **Blair Fennimore**[1,2], **Joseph C. Onyiah**[1,2,3], **Mark E. Gerich**[1,2], **Peter J. Dempsey**[1,4], **Sean P. Colgan**[1,2,3,†]

[1]Mucosal Inflammation Program, University of Colorado Anschutz Medical Campus, Aurora, CO 80045

[2]Department of Medicine, University of Colorado Anschutz Medical Campus, Aurora, CO 80045

[3]Rocky Mountain Regional Veterans Affairs Medical Center, Aurora, CO 80045

[4]Department of Pediatrics, Children's Hospital of Colorado, Aurora, CO 80045.

Abstract

Acute intestinal inflammation includes the early accumulation of neutrophils (PMN). Based on recent evidence that PMN infiltration "imprints" changes in the local tissue environment through local oxygen depletion and the release of adenine nucleotides, we hypothesized that the interaction between transmigrating PMN and intestinal epithelial cells (IECs) results in inflammatory acidification of the tissue. Using newly developed tools, we revealed that active PMN transepithelial migration (TEM) significantly acidifies the local microenvironment, a decrease of nearly 2 pH units. Using unbiased approaches, we sought to define acid-adaptive pathways elicited by PMN TEM. Given the significant amount of adenosine (Ado) generated during PMN TEM, we profiled the influence of Ado on IECs gene expression by microarray and identified the induction

†Correspondence to: Sean P. Colgan, Ph.D., University of Colorado School of Medicine, 12700 East 19th Ave. MS B-146, Aurora, CO 80045, Office phone: 303-724-7235 Fax: 303-724-7243, Sean.Colgan@UCDenver.edu.

*These authors contributed equally to this work.

Author contributions

Ian Cartwright – conceptualization, data curation, formal analysis, validation, investigation, methodology, writing – original draft, review, and editing
Valerie Curtis – Investigation, methodology, writing – review and editing
Jordi Lanis – Resources, methodology
Erica Alexeev – Resources, methodology
Rachel Gao - Resources
Mark Gerich – Resources
Blair Fennimore – Resources
Carlene Chun – Resources
Peter Dempsey – Resources, methodology
Nichole Welch - Resources
Matthew Goldberg – Resources
Rachel Schaefer - Resources
Joseph Onyiah – Resources, methodology
Sean Colgan – Conceptualization, funding acquisition, project administration, writing, review and editing

The authors have declared that no conflict of interest exists

of SLC26A3, the major apical Cl^-/HCO_3^- exchanger in IECs. Utilizing loss- and gain-of-function approaches, as well as murine and human colonoids, we demonstrate that Ado-induced SLC26A3 promotes an adaptive IECs phenotype that buffers local pH during active inflammation. Extending these studies, chronic murine colitis models were used to demonstrate that SLC26A3 expression rebounds during chronic DSS-induced inflammation. In conclusion, Ado signaling during PMN TEM induces an adaptive tissue response to inflammatory acidification through the induction of SLC26A3 expression, thereby promoting pH homeostasis.

Keywords

adenosine; intestinal epithelium; inflammation; neutrophil

INTRODUCTION

Transmigration of neutrophils (PMN, polymorphonuclear leukocytes) to regions of injury is a hallmark of active intestinal inflammation. Without efficient PMN clearance at sites of infiltration, PMN can accumulate and contribute to bystander tissue damage in diseases such as ulcerative colitis (UC) and Crohn's disease (CD). PMN infiltration is accompanied by energy-demanding processes such as migration, phagocytosis, and generation of NADPH oxidase burst and are believed to shift the metabolism of inflamed tissues[1, 2]. For example, recent studies have demonstrated that PMN transepithelial migration (TEM) rapidly depletes microenvironmental O_2, stabilizing hypoxia-inducible factor. This results in an increase in anaerobic glycolysis and induction of multiple targets along the nucleotide metabolism pathway[3, 4]. It has been well established that shifts in glycolysis results in the production of lactic acid, promoting tissue acidification[5–7]. In severe UC it has been observed that colonic pH can drop to values less than 5[4, 7]. PMN appear to be sensitive to changes in extracellular pH[8]. Decreases in extracellular pH (pH 6.5–7) have been shown to stimulate H_2O_2 production, inhibit apoptosis, and extend the functional lifespan of PMN[9]. The major mechanism for regulating tissue pH is through SLC26A3, a transmembrane glycoprotein that transports Cl^- ions across the cell membrane in exchange for HCO_3-[10]. Despite the significance of extracellular acidification, relatively little is known about the mechanisms involved in maintaining tissue pH and how the tissue adapts to changes in extracellular pH during inflammation intestinal inflammation.

During TEM, PMN release significant amount of adenine nucleotides, including ATP, ADP, and dinucleotide polyphosphates (DNP). Through ecto-nucleoside triphosphate diphosphoyhydrolase (NTPDase), ecto-5'-nucleotidase (CD73), and extracellular nucleoside pyrophosphatase/phosphodiesterases (ENPPs), intestinal epithelial cells (IECs) rapidly metabolize ATP, ADP, and DNP into adenosine (Ado)[11–15]. This PMN-derived Ado promotes barrier function in endothelial and epithelial cells of the lung and intestine[16, 17]. Furthermore, activation of the intestinal epithelial A2B Ado receptor (Adora2B) promotes wound healing and improves epithelial barrier during acute colitis[18, 19]. It remains unclear to what extent Ado signaling impacts tissue homeostasis during acute inflammation and how such changes influence disease outcome.

In the present work, we define mechanisms and outcomes of Ado signaling in maintaining cellular homeostasis during PMN TEM. Guided by global mRNA profiling to ascertain the transcriptional impact of Ado on IECs, we hypothesized that Ado signaling is an integral component for adapting to and maintaining extracellular pH balance. Validation studies demonstrated that Ado-induced SLC26A3 expression is CREB/cAMP dependent and increased expression of SLC26A3 significantly limited the shift in extracellular pH following PMN TEM. Moreover, in examining SLC26A3 expression at multiple time points during inflammation in murine colitis models, we show that SLC26A3 is lost in a time-dependent manner during active inflammation, remains decreased during resolution, and ultimately rebounds during chronic inflammation.

Results

Extracellular acidification during PMN transepithelial migration

Tissue acidification is commonly observed during active inflammation[5, 6]. In an effort to understand mechanisms and adaptation to tissue acidification, we developed a model to monitor extracellular pH in real-time during PMN TEM (Fig. 1A). Briefly, T84 IECs were grown to confluency on the underside of 3.0 μm pore permeable supports. A chemotactic agent (1 μM fMLP) was applied to the apical surface (bottom chamber), and 1×10^6 PMN were applied to the basolateral surface (top chamber) to allow for transmigration in the physiologically-relevant basolateral-to-apical direction. Extracellular pH was monitored using a HydroDish and a SDR system which utilizes a fluorescent based pH sensor positioned directly under the T84 IECs [20]. PMN TEM induced a significant decrease in extracellular pH when compared to IECs alone (Fig. 1B, $p<0.01$). To determine if physical contact between activated PMN and the IECs was required for extracellular acidification, T84 IECs were grown to confluency on 0.4 μm pore permeable supports. When grown on the smaller pore inserts there was no significant difference in extracellular pH when comparing IECs alone to IECs in the presence of activated PMN (Fig. 1C). As PMN produce a significant amount of extracellular adenine nucleotides during TEM [21, 22], we extended the study to determine the contribution of Ado signaling in this extracellular acidification. There was no significant difference in extracellular pH when comparing IECs treated with 100 μM Ado to untreated IECs (Fig. 1D, p=not significant). Such findings suggest that Ado-mediated signaling does not drive extracellular acidification. When PMN, in the absence of IECs, where added to the inserts there was no decrease in extracellular pH; however, PMN in the presence of fMLP resulted in a significant decrease in pH (Supp. 1A, $p<0.0001$). The overall decrease in pH observed in the activated PMN, −0.718±0.0090, was not significantly different then the decrease in pH observed in IECs alone, −0.758±0087.

When analyzing the change in pH from non-PMN exposed controls, we see that there is no significant difference in the change in pH when comparing +fMLP, +PMN, Ado exposed, or +PMN/fMLP on 0.4 μM pore inserts (Fig. 1E, −0.28±0.14, −0.39±0.024, −0.23±0.06, and −0.13±0.14 respectively). The change in pH from controls in these 4 conditions was significantly less than the −1.06±0.070 change in pH observed during active PMN TEM (Fig. 1E, $p>0.001$). Finally, the addition of fMLP to PMN alone decreased the extracellular pH by 0.66±0.0090, which is significantly less than the 1.06±0.070 pH decrease seen in

IECs+PMN/fMLP ($p<0.005$). In summary, it is shown that inflammatory acidification requires the TEM of activated PMN.

Extracellular acidification by epithelial-derived lactate

It has been observed that lactate is elevated at sites of inflammation, including UC and CD[23, 24]. To determine the impact of lactate on extracellular acidification we measured secreted lactate levels during the course of PMN TEM. As seen in Figure 1F extracellular lactate significantly increased at 3 hr and remained elevated in the presence of activated PMN, 209 μM±10.17, 317 μM±49.52, 244 μM±29.84 for hr 3, 4, 5 respectively ($p<0.0001$). There was no significant increase in extracellular lactate when T84 IECs were exposed to PMN or fMLP alone when compared to control T84 IECs. To determine the source of lactate, we measured secreted lactate from PMN and PMN+fMLP in the absence of T84 IECs. PMN, regardless of fMLP exposure, produced at most 12.04±2.29 μM lactate (Supp. 1B). This amount of lactate is significantly less than the 50.28±1.41 μM observed in control T84 IECs, $p<0.001$. This indicates that lactate is being produced by the IECs and not PMN during TEM. When T84 IECs were grown on 0.4 μM pore inserts, there was no increase in extracellular lactate following PMN TEM when compared to control T84 IECs (Fig. 1F). These observations indicate that physical PMN/IECs interaction is required for both lactate production and extracellular acidification.

To determine the role of lactate in PMN TEM induced extracellular acidification, we monitored changes in pH with increasing concentrations of lactate (Table 1). From the extrapolated standard curve ($y=7.294–0.001256x-1.461e^{-6}\times^{2}$, with a R squared of 0.9827), we calculated the predicted pH based on lactate concentrations. Based on these calculations, the observed pH in both IECs control and PMN exposed groups was significantly lower than the pH predicted based on observed lactate levels alone (Table 1). These findings indicate that lactic acid production plays a role in extracellular acidification, but is not exclusively responsible for the observed acidification during PMN TEM. This is supported by the observations of lactate independent extracellular acidification in tumors [25, 26].

Epithelial gene expression in response to Ado

PMN TEM has been shown to transcriptionally “imprint” gene expression patterns onto epithelia through localized oxygen depletion and the stabilization of HIF[3]. Given the propensity of PMN to elevate tissue Ado levels during TEM, we sought to gain insight into mechanisms of adaptation to inflammatory acidity mediated by PMN-derived Ado[15, 27]. To do this, we profiled gene expression in T84 IECs exposed to Ado (100 μM) for periods of 3 or 6 hr. As shown in Figure 2A, a principal component analysis revealed prominent separation between treatment groups and tight clustering within individual treatment groups ($p<0.001$). The top induced and repressed genes are highlighted in the heatmap displayed in Figure 2B. Of the top hits from this screen, NR4A2 has previously been characterized as an Ado-responsive gene[28], thereby providing a level of validation for this approach. Likewise, SIK1 has been shown to respond to elevations in cAMP[29] in other cell types. Of significant interest within this Ado-mediated profiling was the highest induced gene SLC26A3, (also called down-regulated in adenoma or DRA), the major Cl^{-}/HCO_3^{-} exchanger expressed on the apical IECs surface[30]. To validate these gene targets, T84 IECs were independently

exposed to Ado (100 μM, 6 hr). As shown in Figure 2C, transcript levels for NR4A2, SIK1, and SLC26A3 were examined by qPCR and revealed that each was significantly increased by exposure to Ado (15.21±0.61, 15.62±1.03, and 7.28±0.74-fold increase compared to vehicle, respectively, each $p<0.001$).

Given the magnitude of PMN-derived Ado observed during PMN TEM and the role of SLC26A3 as a Cl^-/HCO_3^- exchanger, we pursued molecular analysis of the expression and regulation of SLC26A3 by Ado[15]. To further validate SLC26A3 as an Ado responsive gene, T84 IECs were treated with Ado (100 μM) and RNA was collected at 0, 3, 6, 16, and 24 hr. As seen in Figure 2D, transcript levels of SLC26A3 increased at 3 and 6 hr following exposure to Ado (4.02±0.42 and 8.25±0.76-fold increase, $p<0.01$) and returned to baseline by 16 hr. This qPCR analysis was confirmed with protein expression where Ado exposure resulted in a 3.85±0.78-fold increase in SLC26A3 expression with 24 hr treatment with 100 μM Ado (Fig. 2E). To rule out cell line specificity, these results were recapitulated in T84, Caco2, and A549 epithelial cells using a luciferase-based promoter assay. In response to 3 hr treatment with Ado (100 μM), SLC26A3 promoter activity was increased in all cell lines tested (Fig. 2F, each $p<0.01$). Thus, SLC26A3 regulation by Ado appears to be a generalizable response in epithelia cells.

Increased SLC26A3 expression following PMN TEM

To determine SLC26A3 expression following PMN TEM, we examined SLC26A3 expression in T84 IECs 24 hr after PMN TEM. 1×10^6 PMN were migrated across 3.0μm pore inserts in HBSS+HEPES at 37°C, after 24 hr the inserts were collected and washed with PBS to remove PMN. Protein from 4 inserts was pooled for each replicate and SLC26A3 expression was examined by western blot. As seen in Figure 2G, there was a 3.79±0.35 fold increase in SLC26A3 expression in T84 monolayers exposed to activated PMN when compared to T84 monolayers exposed to non-activated PMN. The level of SLC26A3 expression in PMN TEM T84 IECs is similar to SLC26A3 expression in T84 IECs treated with 100 μM Ado for 24 hr (3.79±0.35 and 2.98±0.18 respectively). In addition to analyzing SLC26A3 expression via western blot, SLC26A3 expression was also determined via immunofluorescence (Fig. 2H). SLC26A3 expression and localization appeared similar between Ado treated T84 IECs and T84 IECs following TEM with activated PMN.

Ado-induced SLC26A3 expression is dependent on cAMP/CREB

The Ado A2B receptor has been shown to be the predominant Ado receptor on T84 IECs[31].To confirm this observation, we examined the relative expression of Ado A2A and A2B receptor mRNA. Ado A2B receptor mRNA is expressed 100-fold higher than Ado A2A mRNA in T84 IECs (Fig. 3A, $p<0.0001$). To determine the signaling cascade of Adora2B on SLC26A3 expression, T84 IECs were treated with a combination of the Adora2B inhibitor, PSB-603 (1 μM), and Ado (100 μM) and examined for induction of SLC26A3 by protein expression after 24 hr (Fig. 3B). When analyzed by densitometry, Adora2B-inhibited cells displayed a slight elevation in SLC26A3 expression at baseline (1.58±0.07 fold-increase), but there was no significant increase in SLC26A3 expression following Ado treatment when analyzed by densitometry (1.58±0.07 and 1.59±0.17,

respectively) (Fig. 3B). We speculate that the slight elevation in SLC26A3 expression following PSB-603 treatment is a result of an off-target effect or that PSB-603 is a partial agonist in T84 IECs. The influence of Adora2B inhibition was also assessed using a commercially available SLC26A3 luciferase promoter. In both T84 and Caco2 IECs containing the SLC26A3 luciferase reporter construct, there was no increase in relative luminescence following Ado treatment in cells pre-treated for 1hr with 1μM PSB-603 when compared to vehicle controls (Supp. 2A).

It has been reported previously that forskolin is able to stimulate SLC26A3 expression and activity in a cAMP dependent fashion, we extended these studies to determine the signaling pathway(s) involved in SLC26A3 regulation by Ado[32]. Utilizing pharmacological inhibition, we targeted three significant points within the Ado signaling pathway: namely adenylyl cyclase, CREB, and Erk. We quantified SLC26A3 via mRNA expression in T84 IECs pretreated for 1hr with selective inhibitors followed by a 3hr treatment with Ado (100 μM). Ado induced SLC26A3 expression was significantly inhibited in T84 IECs treated with both the adenylyl cyclase inhibitor and CREB inhibitor; whereas, Erk inhibited T84 IECs had a 13-fold increase in SLC26A3 mRNA expression following treatment with Ado (Fig. 3C). As shown in Figure 3D and Sup 2B, the transcriptional response was validated by protein expression via western blot. T84 IECs pretreated with 1 μM CREB and 10 μM adenylyl cyclase inhibitors had no observable increase in Ado induced SLC26A3 expression at 24 hr when compared to cells treated with the inhibitors alone. Cells pretreated with 30 μM Erk inhibitor had a similar increase in SLC26A3 when compared to vehicle control cells treated with Ado (3-fold). It was noted that Erk inhibition alone had a small influence on SLC26A3 expression and given the extensive cross-talk between MAPK/ERK and cAMP signaling we speculate this increase in SLC26A3 is an off-target effect of the inhibitor[33].

Independent analysis of the SLC26A3 promoter sequence revealed 5 strong CREB binding sites (Fig. 3E). In order to determine the relative contribution of individual CREB sites in the regulation of SLC26A3, each CREB site was mutated independently. Sanger sequencing was utilized to confirm that each CREB site had 4 nucleotides within the CREB binding site mutated, with the exception of CREB5 which had 2 nucleotides altered (Supp. 3B). Both T84 and Caco2 IECs were transfected with the SLC26A3 reporter and baseline SLC26A3 expression was determined. As seen in Figure 3F, in T84 IECs SLC26A3 expression was decreased in promoters containing mutations in CREB sites 2, 3, and 4. In Caco2 IECs, only cells with promoters containing a mutation in the CREB3 site had decreased SLC26A3 expression. To further examine which of the CREB sites are involved in Ado signaling, we examined SLC26A3 expression following Ado treatment (100 μM) in each of the CREB mutants. In both T84 and Caco2 IECs, mutations to the CREB3 site resulted in no increased SLC26A3 expression following Ado treatment; all other CREB mutants displayed a 2–3-fold increase in luminescence when compared to controls (Fig. 3G and Supp. 3C).

SLC26A3 promotes fluid homeostasis

To further understand the role of SLC26A3 in Ado signaling, SLC26A3 was knocked down (KD) using CRISPR approaches or overexpressed (OE) with transduction of a full-length open reading frame (ORF) construct in T84 IECs. SLC26A3 was decreased by 73±1.3% in

the non-clonal KD T84 IECs and increased by 2.50±0.28-fold in the OE T84 IECs (Fig. 4A and B). The KD and OE status of the T84 IECs can also be seen using immunofluorescence (Fig. 4C). As seen in the Ado exposed T84 IECs (Fig 2H), SLC26A3 expression in the OE T84 IECs appears to be predominantly apical, but there is also basal lateral expression as well. Additionally, we validated the increased fluid secretion phenotype observed in SLC26A3 knockout mice in our SLC26A3 KD cell line by monitoring Ado and forskolin associated fluid flux[34]. SLC26A3 KD cells showed significant increases in fluid transport from the basal to apical compartment following both Ado (100 μM) and forskolin (10 μM) treatment when compared to both vector controls (Supp. 4A&B $p<0.0001$). Interestingly, the Ado associated fluid flux observed in SLC26A3 OE cells was not only decreased, but there was a net flux of 14.44±3.85μL/cm^2 from the apical to basal compartment ($p<0.001$).

To examine the effect of SLC26A3 expression on chloride secretion the peak short-circuit current (Isc) was calculated following treatment with Ado. When the basal surface was exposed to Ado, decreased expression of SLC26A3 did not alter peak Isc when compared to vector controls. However, SLC26A3 OE cells had a significant increase in peak Isc with a 1.86±0.085-fold change compared to vector control, when treated with Ado (30 μM) (Supp. 4C). Next, Ado was applied to the apical side of the inserts and the Isc was measured. As seen in the basally treated cells, SLC26A3 OE cells had an increase in peak Isc. Interestingly, SLC26A3 KD cells also had a significant increase in peak Isc when compared in vector controls treated with 30 μM Ado on the apical surface (Supp. 4D, $p<0.001$). When comparing the OE and KD cells, the OE cells have a larger Isc response to apical application of 30 μM Ado than the KD cells ($p<0.001$).

SLC26A3 maintains pH homeostasis during PMN transmigration

Based on SLC26A3's role as a Cl−/bicarbonate transporter and regulator of colonic pH, we next determined the influence of SLC26A3 expression on pH regulation during PMN TEM. As previously described, PMN were transmigrated across confluent SLC26A3 OE, KD, 100 μM Ado pretreated, and T84 vector/vehicle control monolayers. As seen in Figures 4D–F, SLC26A3 expression had a significant influence on extracellular pH. The extracellular pH decreased by 2.02±0.025 in SLC26A3 KD cell lines, which was significantly lower than vector controls ($p<0.001$) (Fig. 4D). While the extracellular pH in SLC26A3 OE cells decreased in the during PMN TEM, the difference in extracellular pH between PMN exposed and unexposed inserts was significantly less than the change observed in the vector control cells (Figure 4G, $p<0.01$). T84 IECs pretreated with Ado for 24 hr had a similar response to PMN TEM as the OE cells. The overall decrease in pH observed in Ado pretreated cells was −1.38±0.093, which is 0.3379±0.093 lower than the vehicle controls ($p<001$).

These studies were extended to investigate how SLC26A3 expression impacts intracellular pH. Using BCECF-am we monitored intracellular pH following Ado treatment over the course of 120 min. When analyzing the change in pH between T0 and T120 min, elevated expression of SLC26A3 greatly attenuated the intracellular acidification observed in both the vector control and KD cells when treated with both 10 and 100 μM Ado ($p<0.001$) (Fig.

4H). SLC26A3 KD cells displayed a similar decrease in intracellular when compared to vector control cells. When using 10 μM forskolin similar results were observed (Supp. 4E).

Adenosine induces fluid flux in mouse intestinal colonoids

We next sought to examine the impact of Ado on a non-transformed cell line. Here, colonoids derived from the colon of C57BL/6 mice were treated with Ado (100 μM) or forskolin (10 μM). As shown in Figure 5 A&B, forskolin induced detectable fluid flux (reflected as an increase in colonoid size) at 6 and 24 hr. Ado-induced fluid accumulation was detectable at 24 hr. Given this response, we examined SLC26A3 expression in the murine colonoids by qPCR. Similar to responses in transformed cell lines, Ado (100 μM, 3 hr) induced a significant increase in SLC26A3 in murine colonoids compared to vehicle controls (Fig. 5C, $p < 0.01$). Extending these studies, we exposed human derived colonoids to 100 μM Ado for 3 hr and examined SLC26A3 and NR4A2 expression by qPCR. As seen in Figure 5D Ado significantly induced the relative expression of both SLC26A3 and NR4A2 in the normal human colonoids (4.43±1.08 and 8.49±2.17, $p<0.005$ and $p<0.0001$). As a positive control for cAMP/CREB response, human colonoids were treated with 10μM forskolin for 3 hr and qPCR was used to measure the expression of several CREB responsive genes, SLC26A3, cFOS, NR4A2, and NR4A3[32, 35]. There was a significant increase in all genes tested following treatment with forskolin (Supp. 4F, $p<0.001$).

SLC26A3 dysregulation in Inflammatory Bowel Disease

We then examined SLC26A3 expression in human tissues using biopsies from CD, active UC, inactive UC patients, and healthy controls. Immunostaining for SLC26A3 was done to examine SLC26A3 expression (Fig. 5E). In healthy colons, there was a high degree of apical IECs expression of SLC26A3. This pattern was aberrant (Fig. 5E, red arrows) and SLC26A3 expression was significantly repressed in both active and inactive UC and CD when compared to healthy controls (Fig. 5F, $p<0.001$). Despite an overall decrease in SLC26A3 expression in UC patients, we observed regions of the colon that had similar expression levels and localization as healthy controls (Fig. 5E&F). This relatively “normal” SLC26A3 expression was seen in all 4 active UC and 4 inactive UC patients. These regions of increased SLC26A3 expression was absent in the CD patients.

SLC26A3 expression in murine models of colitis

It has been well established that SLC26A3 expression is repressed in DSS induced colitis. However, it has not been well documented at what point during the development of colitis that SLC26A3 expression is lost. To determine the kinetics of SLC26A3 loss, we treated mice with 3% DSS and collected cohorts at days 1, 3, 5, and 7. As seen in Figure 6A, SLC26A3 expression, as determined by the fluorescent ratio of SLC26A3:DAPI, begins to diminish after 3 days of DSS treatment and continues to decrease at days 5 and 7 when compared to control mice (0.45±0.040, 0.3589±0.038, 0.25±0.053, and 0.82±0.015 respectively, p-value<0.02 for all comparisons). The staining pattern of SLC26A3 begins to change starting at day 3 (Fig. 6B, red arrow), the expression of SLC26A3 begins to move from being expressed exclusively on the apical surface to being both apically expressed and expressed in the cytoplasm. Additionally, SLC26A3 can be seen being expressed in the crypt of the villus, which is not seen in control mice.

To examine SLC26A3 expression in the context of chronic inflammation, we utilized a chronic DSS murine model[36]. Mice were treated with 3% DSS for 7 days followed by 3 weeks of water before undergoing a second and third round of DSS treatment. Cohorts of mice were collected after the first, second, and third round of DSS. When epithelial SLC26A3 expression was examined in the context of chronic DSS we observed expression increasing after each subsequent round of DSS treatment (Fig. 6C). We see the relative expression of SLC26A3, as measured by SLC26A3 fluorescent intensity normalized to DAPI intensity, significantly lower after the first round of DSS when compared to controls (0.27±0.024 and 0.84±0.063, $p<0.0001$). After the second round of DSS, SLC26A3 expression increases over 3-fold when compared to SLC26A3 expression after round 1 (0.61±0.04 and 0.27±0.024 respectively, $p<0.0004$). SLC26A3 expression continues to increase following the third round of DSS (1.016±0.10). SLC26A3 expression after the third round of DSS is similar to expression seen in control mice, however, the expression pattern seen after the third round of DSS is very different. As seen in Figure 6D, there are regions of the colon with SLC26A3 expression patterns similar to controls and regions with diffuse cytoplasmic staining. In addition, SLC26A3 staining is observed in the crypts and in transverse sections, which is not observed in control mice (Fig. 6D, red arrows).

DISCUSSION

An understanding of the metabòlic responses to inflammation is an area of significant interest. Recent studies, for example, have implicated shifts in tissue metabolism as important clues that determine the overall outcomes of inflammatory responses[37]. Of particular interest in the mucosa is the adaptation to “inflammatory hypoxia”, wherein oxygen depletion generated by the PMN oxidative burst “imprints” the initiation of an inflammatory resolution program through the stabilization of HIF[3]. In this regard, a consistent finding in inflammatory hypoxia is the generation of high levels of extracellular nucleotides[38]. Despite our understanding of extracellular adenine nucleotide metabolism[11–15] and the protective nature of Ado in colitis[18, 19], there remains significant gaps in our understanding of the mechanism(s) by which Ado promotes inflammatory resolution. The present study provides significant new insight into Ado-mediated control of what we have termed “inflammatory acidification” during active inflammation.

A common feature of many inflammatory sites is tissue acidification. The primary mechanism of acidification is thought to include increased accumulation of lactic acid resulting from enhanced glycolysis. Physiological lactate concentrations are actively maintained in the range of 1.5–3mM in blood and tissues of healthy individuals[39]. During active inflammation, local lactate levels can exceed 10mM (e.g. in rheumatic synovial fluid) and can increase to as high as 30–40mM in some cancerous tissues[39]. Other studies have shown that that tissue pH can fall to as low as 3 at sites of inflammation (e.g. active IBD)[4]. Given these observations, we developed a model to study changes in extracellular pH in real time. This analysis revealed that transmigrating PMN significantly decrease extracellular pH in the presence of T84 IECs. It is notable that the largest changes in pH were observed during active transmigration, the decrease in pH was attenuated when the IECs where grown on inserts which prevents PMN-epithelial contact. This observation suggests that direct interactions between PMN and epithelia is necessary for inflammatory acidification. Likely

this response reflects the rapid induction of epithelial glycolysis elicited by HIF stabilization within the epithelium[3]. Based on the observations that PMN TEM stabilizes HIF, which rapidly induces glycolysis, we monitored extracellular lactate. This analysis revealed significant secretion of lactic acid by IECs, requiring direct interaction between the IECs and active PMN. Further investigations determined that the decrease in pH observed during PMN TEM was larger than what was predicted based on the lactic acid concentrations observed during PMN TEM. This suggests that lactic acid production is not solely responsible for the extracellular acidification observed during PMN TEM. These findings are supported by observations made in tumor microenvironments. It has been reported that lactic acid production accounts from 30–60% of the acidification observed in tumors[26, 40, 41].

Considering the prominent role of adenine nucleotide signaling during PMN TEM[22], we defined the influence of Ado signaling on gene regulation. Guided by an unbiased transcriptional profiling of Ado treated IECs, we identified the prominent induction of SLC26A3 by Ado. We also observed increased SLC26A3 expression in T84 IECs following PMN TEM. SLC26A3 is a transmembrane glycoprotein that transports chloride ions across the cell membrane in exchange for bicarbonate ions[10]. Mutations resulting in loss of SLC26A3 expression are associated with congenital chloride diarrhea (CLD)[42]. In addition to being associated with CLD, SLC26A3 is dysregulated in intestinal inflammation[43, 44] and DSS colitis severity is increased in SLC26A3$^{-/-}$ mice[34, 45]. Both *in vivo* and *in vitro* SLC26A3 dysregulation has been associated with decreased bicarbonate secretion and chloride absorption, but not chloride secretion[46, 47]. In addition, SLC26A3 has been reported to be regulated by intracellular pH, as well as, potentially plays a role in regulating extracellular pH in the colon, SLC26A3−/− mice have a slightly more acidic colons than wild type controls[47, 48]. Consistent with prior research, SLC26A3 KD cell lines did not exhibit changes in short-circuit current, an indicator of chloride secretion.

To gain insight into the role of SLC26A3 in pH regulation during PMN TEM, we investigated loss and gain of SLC26A3 function in the maintenance of extracellular and intracellular pH. Our studies demonstrate that increased SLC26A3 expression significantly limits extracellular acidification observed during PMN TEM. When SLC26A3 was lost, the shift in pH was exacerbated providing evidence that this Ado-induced SLC26A3 plays an adaptive role in our inflammatory *in vitro* model. Given the multiple health issues associated with SLC26A3-null mice (e.g. high Cl^- content diarrhea, growth retardation and volume depletion) [47], we elected to extend our analysis to define SLC26A3 expression in human inflammatory bowel disease patients. We confirmed previous findings that SLC26A3 expression is decreased in active UC patients[43, 49], and also show decreased expression in individuals with inactive UC and in the colon of CD patients. In both active and inactive UC patients we observed patchy regions of the colon which expressed SLC26A3 to a level similar to healthy patients. Interestingly, these regions of increased SLC26A3 expression were not seen in CD patients. While UC and CD are related but distinct diseases, we do not know the nature of these differences in SLC26A3 expression. Likely they reflect some differences in the tissue microenvironment (e.g. cytokines, microflora, other inflammatory mediators), studies that will require significant work to understand.

Using immunohistochemical approaches, we not only confirmed that SLC26A3 expression was decreased in the DSS murine model of mucosal inflammation, but also expanded upon these observations to show the time course of SLC26A3 loss in DSS colitis as well as expression patterns in chronic murine models. The increase in SLC26A3 expression observed in chronic DSS colitis supports our observations that SLC26A3 expression is an adaptive phenotype in response to inflammatory acidity. While limited, however, there is evidence which suggests the PMN infiltration increases with each subsequent round of DSS, supporting the idea that PMN influence the expression of SLC26A3[53, 54]. We speculate that this phenotype represents an adaptive phenotype wherein tissues respond to inflammatory acidification by adapting over longer periods of inflammation (e.g. changes in the inflammatory mediator milieu changes that favor expression of SLC26A3). Our observations made *in vitro* that PMN TEM significantly induces SLC26A3 expression also supports the possibility that PMN-associated nucleotide signaling could be relevant in the regulation of SLC26A3 in the *in vivo* setting. This premise is supported by our previous observation that PMN accumulation is strongly associated with HIF stabilization and HIF target gene induction (e.g. GLUT1) in patients with active IBD[3]. In this regard, it is notable that a number of gene products along the adenine nucleotide metabolism and signaling cascade are direct transcriptional targets of HIF[55]. Thus, it is possible that HIF could contribute fundamentally to the regulation of SLC26A3 by PMN-derived nucleotides.

Taken together, these results provide new molecular insight into the role of PMN signaling during active inflammation. Our results highlight, for the first time, an Ado-mediated adaptive tissue response that buffers inflammatory acidification. SLC26A3 promotes an adaptive tissue response, thereby limiting the shifts in pH following PMN TEM. Like previous work highlighting HIF signaling, the present observations implicate transcriptional imprinting of Ado signaling in which transmigration provides mucosal memory after the clearance of PMN and elicits functional resolution responses important for tissue homeostasis.

METHODS

PMN isolation and stimulation

Human neutrophils were isolated from whole venous blood of healthy volunteers as described in detail previously[56] (IRB# 06–0853). Briefly, whole venous blood was collected in syringes containing anticoagulant (K_2EDTA at 1.8mg/ml blood). Blood was gently layered over double-density Histopaque gradients (1119 / 1077) and centrifuged at 700 × *g* in a swinging bucket rotor centrifuge for 30min without brake. The resulting granulocyte layer was collected and residual red blood cells lysed. PMN were washed with ice-cold HBSS- (w/out $CaCl_2$ or $MgCl_2$), counted and used within 2 hr of isolation.

Cell culture

T84 (#CCL-248; American Type Culture Collection (ATCC), Manassas, VA), Caco2 (#HTB-37; ATCC), and A549 (#CCL-185; ATCC) human epithelial cell lines were obtained from ATCC and were cultured in 95% air with 5% CO_2 at 37°C according to instructions provided by ATCC. Where indicated, cells were cultured on 3.0 μM or 0.4 μm pore polyester

transwell inserts for 10–14 days to obtain confluent cell monolayers as measured by transepithelial resistance (CoStar, Cambridge, MA). Ado (100μM) and foskolin (10μM) from Sigma-Aldrich (St. Louis, MO) were added to sterile filtered HBSS or DMSO respectively (Sigma-Aldrich). ERK activation inhibitor Peptide I (30μM), CREB inhibitor (1μM), 666–15, adenylate cyclase inhibitor (10μM), 2',5'-dideoxyadenosine, and adenosine A2B receptor inhibitor (10μM), PSB-603, from Sigma-Aldrich were added to sterile DMSO (Sigma-Aldrich). Mouse colonoids created from mouse IECs were isolated from the colons of C57BL/6 mice as previously described[57]. Human colonoids were harvested and cultured as previously described [58]. Briefly, colonoids were suspended in Matrigel (Corning) and plated into 6-well plates, each well contains four 25μl Matrigel bubble overlaid with 1ml of complete media. Complete human colonoid media (WENRAS) and complete mouse colonoid media (WENR) was prepared as previously described[59, 60]. Lentiviral particles encoding the SLC26A3 ORF (Origene, Rockville, MD, USA) were transduced into T84 IECs using established protocols to derive SLC26A3-overexpression (SLC26A3-OE; and empty vector or EV) cell lines. Knockdown cell lines were created using a single-guide RNA (sgRNA) sequence targeting the gene was generated by the Functional Genomic Core at the University of Colorado Denver. The sgRNA sequence used to target SLC26A3 was 5'-GCCGAAAAGGTAGATTA-3'. The sgRNA oligos were ligated into the lentiCRISPR v2 vector[61] which co-express cas9 and sgRNA in the same vector. The CRISPR lentivirus vector was then packaged according to a standard protocol. To produce lentiviral vectors, lentiviral plasmids with the target sgRNA were transduced into HEK293T cells together with second-generation packaging plasmids (psPAX2 and pMD2.G) following previously published procedures[62]. The collected virus was placed on 60–70% confluent T84 IECs along with 10ug/ml polybrene and incubated for 24 hr. After 24 hr the media was replaced with fresh M4 and incubated for another 24 hr. M4 containing 6 μg/ml puromycin was added to the cells. After 7 days of selection cells were collected and assayed for SLC26A3 knockout via western blot.

To measure agonist-stimulated short circuit currents (Isc), transepithelial potentials and electrical resistances were monitored on a commercially available voltage clamp (EVOHM2,World Precision Instruments, Sarasota,FL) interfaced with an equilibrated pair of calomel electrodes, as described in detail elsewhere[63]. For each experiment we averaged the data collected from 4 technical replicates. T84 IECs grown on inserts and the net fluid movement was measured as described previously[64], with minor modifications, following application of 100 μM Ado or 10 μM forskolin to the apical compartment. In brief, the apical solution of confluent T84 IECs monolayers grown on 0.33 cm^2 permeable supports was replaced with 60 μl of media and layered with 60 μl of warm, sterile mineral oil to minimize evaporation as previously described[64]. After 24 hr, the apical solution was collected, centrifuged at 10,000 X g, quantified with a calibrated pipette and weighed on a balance (Sartorius, Inc., Bohemia, NY). For each experiment we averaged the data collected from 4 technical replicates.

Measurement of intra- and extracellular pH

To measure real-time changes in intracellular pH a BCECF-am assay was utilized based on limited leakage of the BCECF following the cleavage of the acetoxymethyl ester by

cytosolic esterases and ability to monitor intracellular pH over an extended period of time [65, 66]. Confluent T84 IECs grown on 0.33 cm^2 permeable supports were loaded with 1 μM BCECF-am (ThermoFisher) in HBSS with $HCO3^-$ for 60 minutes at 37°C. After washing in HBSS with HEPES, the cells were treated with Ado (10 or 100 μM) or forskolin (10 μM). Using a Synergy H1 microplate reader (Biotek) the dual-excitation ratio with λ1 = 490 nm and λ2 = 440 nm and fixed emission at 535 nm was measured every minute for 2 hr at 37°C under atmospheric CO2 levels. pH valúes were calculated based on values obtained from a standard curve generated each run per standard protocol provided by ThermoFisher. For each experiment we averaged the data collected from 4 technical replicates.

To measure real-time changes in extracellular pH HydroDish HD24 (PreSens Precision Sensing, Regensburg, Germany) and a SDR SensorDish Reader (PreSens Precision Sensing) were utilized. Briefly, T84 IECs were grown to confluence on the underside of Transwell 3.0 μm or 0.4 μm pore permeable supports. The inserts were placed into HBSS with $HCO3^-$ and without HEPES. 1 μM fMLP was added to the apical (bottom) chamber immediately prior to the addition of 1×10^6PMN to the basolateral side (top) and the pH was monitored every minute for 400 minutes at 37°C under atmospheric CO2 levels. The extracellular pH was also determined with PMN alone and T84 treated with 100 μM Ado on the basolateral surface. For each experiment we averaged the data collected from 4 technical replicates.

Animal Studies

C57BL/6 mice (The Jackson Laboratory) were bred in-house. All animals were handled according to protocols approved by the institutional committee for animal use. Gender, age, and weight-matched mice were used in DSS studies. DSS (36,000–50,000 MW; MP Biomedicals, Colon, OH) was added to drinking water (3%), followed by monitoring for weight loss over 7 days. Cohorts of 4 mice were collected on day 1, 3, 5, and 7. For chronic DSS, 3% DSS was added to drinking water, followed by monitoring for weight loss over 7 days. DSS was replaced with water for 21 days before adding 3% DSS to the drinking water for another 7 days. This was repeated for a third round. Cohorts of 4 mice were collected after the first, second, and third round of DSS. Post-mortem colons were harvested by blunt dissection and the distal 2 cm collected and fixed in 10% buffered-formalin (Sigma-Aldrich) prior to paraffin imbedding and staining for immunofluorescence. Four mice were used for each experimental group.

Human Samples

Slide mounted parafilm embedded tissue samples from healthy controls, active UC, inactive UC, and CD, identified by a pathologist, were obtained from the University of Colorado Biorepository (IRB# 14–2012). There were four patients in each group.

Microarray and Analysis

T84 IECs were plated on large (5 cm^2, 0.4 μm permeable polyester) inserts (Corning, Corning, NY, USA) and grown to resistance. The inserts were then washed and equilibrated in Hanks balanced salt solution with Ca^{2+} (HBSS+, Sigma-Aldrich) and treated apically and basolaterally with 100 μM adenosine for 3 or 6 hr. The cells were collected in TRIzol (Thermo Fisher Scientific) for RNA isolation and gDNA clean-up (Qiagen, Hilden,

Germany). A hybridization cocktail was prepared starting with 100 ng total RNA using the GeneChip WT PLUS Reagent Kit (Thermo Fisher Scientific). The samples were hybridized to the arrays for 16 hr at 45°C in a GeneChip Hybridization Oven 645 (Thermo Fisher Scientific). Then, the arrays were washed and stained in a GeneChip Fluidics Station 450 (Thermo Fisher Scientific) and scanned in a GeneChip Scanner 3000 (Thermo Fisher Scientific). Each condition was performed in triplicate. The data were analyzed as gene expression (fold change) at 3 and 6 hr over expression in untreated cells. Principal component analysis was performed with XLSTAT (Addinsoft, Inc, Paris, France).

Measurement of lactic acid production

To measure lactic acid produced during PMN TEM a commercially available colorimetric L-lactate assay kit was utilized (AAT Bioquest, Sunnyvale, CA). 1×10^6 PMN were migrated across T84 monolayers grown on 0.4 or 3.0 μM pore inserts. Supernatant from the apical surface was collected at various time points during PMN TEM. For each experiment we averaged the data collected from 4 technical replicates.

Transcriptional analysis

TRIzol reagent (Invitrogen) was used to isolate RNA from T84 IECs. RNAeasy Plus (Qiagen) was used to isolate RNA from mouse colon tissue. cDNA was reverse transcribed using the iScript cDNA Synthesis Kit (Bio-Rad, Hercules, CA, USA). PCR analysis was performed using SYBR Green (Applied Biosystems, Carlsbad, CA, USA) and the primer sequences are listed in Table 2. Each experiment was performed in triplicate.

Protein analysis and immunofluorescence

Whole cell lysates were extracted into RIPA buffer with protease inhibitor (Roche). Lysates were spun at max RPM for 45 min at 4°C. Supernatant was collected and quantified for normalization using Pierce BCA protein assay kit (Thermo Fisher Scientific). Than 4x Laemmli sample buffer (Bio-Rad) with 2-mercaptoethanol was added. Samples were not boiled and 20 μg lysate per well was used. Western blotting of these lysates was performed using rabbit polyclonal anti-SLC26A3 ab83545 (Abcam, Cambridge, MA, USA) and rabbit polyclonal anti-β-actin (Abcam, Cambridge, UK).

To localize and quantify SLC26A3 expression paraffin fixed human and mouse colon tissue was processed for microscopy as described[18]. Both human and mouse samples were stained with rabbit polyclonal anti-SLC26A3 ab244452 (Abcam) followed by Alexa Fluor 488 anti-rabbit secondary Ab (Invitrogen) and counter stained with ProLong Gold Antifade with DAPI (Thermo Scientific).

Luciferase reporter assay

T84, Caco2, and A549 cells at ~60–70% confluency were transfected with 200–400 ng of SLC26A3 *Renilla* luciferase (Switchgear genomics, Carlsbad, CA) and 20–100 ng control *Firefly* luciferase plasmids (Promega, Madison, WI). Transfection was performed using Lipofectamine 3000™ reagent (Invitrogen) according to manufactures instructions. After 24 hr, triplicate wells were treated with vehicle, Ado (100 μM), A2B inhibitor (PSB-603, 1 μM), CREB inhibitor (666–15, 1 μM), 2',5'-dideoxyadenosine (5 μM), or Erk inhibitor (30

μM) for 2 hr. Cell lysis was performed with Passive Lysis Buffer (Promega) and assayed using a Dual-Luciferase® Reporter Assay (Promega) on a GloMax Multidection System (Promega). SLC26A3 *Renilla* signal was normalized to the control *Firefly* signal to account for transfection efficiency.

The 5 CREB sites identified in the SLC26A3 promoter were mutated using QuikChange Lightening Site-Directed Mutagenesis Kit (Agilent Technology, Santa Clara, CA). Primer sequences used are identified in Supp. 1. CREB site mutations were confirmed by Sanger sequencing. Purified plasmid was sent to Quintarabio (San Francisco, CA) and sequenced using the primer 5'-CTAGCAAAATAGGCTGTCCC-3'.

Statistical analysis

Data are expressed as mean valúes ± SEM. Data were analyzed with Student's t test between two groups or analysis of variance (ANOVA) coupled with post hoc Bonferroni test for multiple pairwise comparisons. Probability valúes of $p < 0.05$ were considered statistically significant.

Supplementary Material

Refer to Web version on PubMed Central for supplementary material.

Acknowledgments

This work was supported by NIH grants DK1047893, DK50189, DK095491, DK103712 and by the Veterans Administration Merit Award BX002182.

REFERENCES

1. Chin AC, Parkos CA. Pathobiology of neutrophil transepithelial migration: implications in mediating epithelial injury. Annu Rev Pathol 2007; 2: 111–143. [PubMed: 18039095]
2. Kominsky DJ, Campbell EL, Colgan SP. Metabolic shifts in immunity and inflammation. J Immunol 2010; 184(8): 4062–4068. [PubMed: 20368286]
3. Campbell EL, Bruyninckx WJ, Kelly CJ, Glover LE, McNamee EN, Bowers BE et al. Transmigrating neutrophils shape the mucosal microenvironment through localized oxygen depletion to influence resolution of inflammation. Immunity 2014; 40(1): 66–77. [PubMed: 24412613]
4. Roediger WE, Lawson MJ, Kwok V, Grant AK, Pannall PR. Colonic bicarbonate output as a test of disease activity in ulcerative colitis. J Clin Pathol 1984; 37(6): 704–707. [PubMed: 6327778]
5. Wike-Hooley JL, Haveman J, Reinhold HS. The relevance of tumour pH to the treatment of malignant disease. Radiother Oncol 1984; 2(4): 343–366. [PubMed: 6097949]
6. Fiddian-Green RG. Gastric intramucosal pH, tissue oxygenation and acid-base balance. Br J Anaesth 1995; 74(5): 591–606. [PubMed: 7772437]
7. Nugent SG, Kumar D, Rampton DS, Evans DF. Intestinal luminal pH in inflammatory bowel disease: possible determinants and implications for therapy with aminosalicylates and other drugs. Gut 2001; 48(4): 571–577. [PubMed: 11247905]
8. Percival SL, McCarty S, Hunt JA, Woods EJ. The effects of pH on wound healing, biofilms, and antimicrobial efficacy. Wound Repair Regen 2014; 22(2): 174–186. [PubMed: 24611980]
9. Trevani AS, Andonegui G, Giordano M, Lopez DH, Gamberale R, Minucci F et al. Extracellular acidification induces human neutrophil activation. J Immunol 1999; 162(8): 4849–4857. [PubMed: 10202029]

10. Lamprecht G, Heil A, Baisch S, Lin-Wu E, Yun CC, Kalbacher H et al. The down regulated in adenoma (dra) gene product binds to the second PDZ domain of the NHE3 kinase A regulatory protein (E3KARP), potentially linking intestinal Cl−/HCO3− exchange to Na+/H+ exchange. Biochemistry 2002; 41(41): 12336–12342. [PubMed: 12369822]
11. Colgan SP, Taylor CT. Hypoxia: an alarm signal during intestinal inflammation. Nat Rev Gastroenterol Hepatol 2010; 7(5): 281–287. [PubMed: 20368740]
12. Colgan SP, Eltzschig HK. Adenosine and hypoxia-inducible factor signaling in intestinal injury and recovery. Annu Rev Physiol 2012; 74: 153–175. [PubMed: 21942704]
13. Linden J Molecular approach to adenosine receptors: receptor-mediated mechanisms of tissue protection. Annu Rev Pharmacol Toxicol 2001; 41: 775–787. [PubMed: 11264476]
14. Colgan SP, Eltzschig HK, Eckle T, Thompson LF. Physiological roles for ecto-5'-nucleotidase (CD73). Purinergic Signal 2006; 2(2): 351–360. [PubMed: 18404475]
15. Curtis VF, Cartwright IM, Lee JS, Wang RX, Kao DJ, Lanis JM et al. Neutrophils as sources of dinucleotide polyphosphates and metabolism by epithelial ENPP1 to influence barrier function via adenosine signaling. Mol Biol Cell 2018; 29(22): 2687–2699. [PubMed: 30188771]
16. Colgan SP, Campbell EL, Kominsky DJ. Hypoxia and Mucosal Inflammation. Ann Rev Pathol 2016; 11: 77–100. [PubMed: 27193451]
17. Colgan SP, Eltzschig HK. Adenosine and hypoxia-inducible factor signaling in intestinal injury and recovery. Annu Rev Physiol 2012; 74: 153–175.. [PubMed: 21942704]
18. Aherne CM, Saeedi B, Collins CB, Masterson JC, McNamee EN, Perrenoud L et al. Epithelial-specific A2B adenosine receptor signaling protects the colonic epithelial barrier during acute colitis. Mucosal Immunol 2015; 8(6): 1324–1338. [PubMed: 25850656]
19. Aherne CM, Kewley EM, Eltzschig HK. The resurgence of A2B adenosine receptor signaling. Biochim Biophys Acta 2011; 1808(5): 1329–1339. [PubMed: 20546702]
20. Naciri M, Kuystermans D, Al-Rubeai M. Monitoring pH and dissolved oxygen in mammalian cell culture using optical sensors. Cytotechnology 2008; 57(3): 245–250. [PubMed: 19003181]
21. Hall CHT, Campbell EL, Colgan SP. Neutrophils as Components of Mucosal Homeostasis. Cell Mol Gastroenterol Hepatol 2017; 4(3): 329–337.. [PubMed: 28884136]
22. Colgan SP. Neutrophils and inflammatory resolution in the mucosa. Semin Immunol 2015; 27(3): 177–183. doi: 10.1016/j.smim.2015.1003.1007. Epub 2015 Mar 1026.
23. Haas R, Smith J, Rocher-Ros V, Nadkarni S, Montero-Melendez T, D'Acquisto F et al. Lactate Regulates Metabolic and Pro-inflammatory Circuits in Control of T Cell Migration and Effector Functions. PLoS Biol 2015; 13(7): e1002202. [PubMed: 26181372]
24. Hove H, Mortensen PB. Influence of intestinal inflammation (IBD) and small and large bowel length on fecal short-chain fatty acids and lactate. Dig Dis Sci 1995; 40(6): 1372–1380. [PubMed: 7781463]
25. Yamagata M, Hasuda K, Stamato T, Tannock IF. The contribution of lactic acid to acidification of tumours: studies of variant cells lacking lactate dehydrogenase. Br J Cancer 1998; 77(11): 1726–1731. [PubMed: 9667639]
26. Newell K, Franchi A, Pouyssegur J, Tannock I. Studies with glycolysis-deficient cells suggest that production of lactic acid is not the only cause of tumor acidity. Proc Natl Acad Sci U S A 1993; 90(3): 1127–1131. [PubMed: 8430084]
27. Lennon PF, Taylor CT, Stahl GL, Colgan SP. Neutrophil-derived 5'-adenosine monophosphate promotes endothelial barrier function via CD73-mediated conversion to adenosine and endothelial A2B receptor activation. J Exp Med 1998; 188(8): 1433–1443. [PubMed: 9782120]
28. Zhang L, Paine C, Dip R. Selective regulation of nuclear orphan receptors 4A by adenosine receptor subtypes in human mast cells. J Celi Commun Signal 2010; 4(4): 173–183.
29. Lee J, Tong T, Takemori H, Jefcoate C. Stimulation of StAR expression by cAMP is controlled by inhibition of highly inducible SIK1 via CRTC2, a co-activator of CREB. Mol Cell Endocrinol 2015; 408: 80–89. [PubMed: 25662274]
30. Bhutia YD, Babu E, Ramachandran S, Yang S, Thangaraju M, Ganapathy V. SLC transporters as a novel class of tumour suppressors: identity, function and molecular mechanisms. Biochem J 2016; 473(9): 1113–1124.. [PubMed: 27118869]

31. Strohmeier GR, Reppert SM, Lencer WI, Madara JL. The A2b adenosine receptor mediates cAMP responses to adenosine receptor agonists in human intestinal epithelia. J Biol Chem 1995; 270(5): 2387–2394. [PubMed: 7836474]
32. Tse CM, Yin J, Singh V, Sarker R, Lin R, Verkman AS et al. cAMP Stimulates SLC26A3 Activity in Human Colon by a CFTR-Dependent Mechanism That Does Not Require CFTR Activity. Cell Mol Gastroenterol Hepatol 2019; 7(3): 641–653. [PubMed: 30659943]
33. Dumaz N, Marais R. Integrating signals between cAMP and the RAS/RAF/MEK/ERK signalling pathways. Based on the anniversary prize of the Gesellschaft fur Biochemie und Molekularbiologie Lecture delivered on 5 July 2003 at the Special FEBS Meeting in Brussels. FEBS J 2005; 272(14): 3491–3504.
34. Xiao F, Yu Q, Li J, Johansson ME, Singh AK, Xia W et al. Slc26a3 deficiency is associated with loss of colonic HCO3 (−) secretion, absence of a firm mucus layer and barrier impairment in mice. Acta Physiol (Oxf) 2014; 211(1): 161–175. [PubMed: 24373192]
35. Conkright MD, Guzman E, Flechner L, Su AI, Hogenesch JB, Montminy M. Genome-wide analysis of CREB target genes reveals a core promoter requirement for cAMP responsiveness. Mol Cell 2003; 11(4): 1101–1108. [PubMed: 12718894]
36. Wirtz S, Neufert C, Weigmann B, Neurath MF. Chemically induced mouse models of intestinal inflammation. Nat Protoc 2007; 2(3): 541–546. [PubMed: 17406617]
37. Taylor CT, Colgan SP. Regulation of immunity and inflammation by hypoxia in immunological niches. Nat Rev Immunol 2017; 17(12): 774–785.. [PubMed: 28972206]
38. Eltzschig HK, Sitkovsky MV, Robson SC. Purinergic signaling during inflammation. N Engl J Med 2012; 367(24): 2322–2333. [PubMed: 23234515]
39. Pucino V, Bombardieri M, Pitzalis C, Mauro C. Lactate at the crossroads of metabolism, inflammation, and autoimmunity. Eur J Immunol 2017; 47(1): 14–21. [PubMed: 27883186]
40. Mookerjee SA, Goncalves RLS, Gerencser AA, Nicholls DG, Brand MD. The contributions of respiration and glycolysis to extracellular acid production. Biochim Biophys Acta 2015; 1847(2): 171–181. [PubMed: 25449966]
41. Kato Y, Ozawa S, Miyamoto C, Maehata Y, Suzuki A, Maeda T et al. Acidic extracellular microenvironment and cancer. Cancer Cell Int 2013; 13(1): 89. [PubMed: 24004445]
42. Hoglund P, Haila S, Socha J, Tomaszewski L, Saarialho-Kere U, Karjalainen-Lindsberg ML et al. Mutations of the Down-regulated in adenoma (DRA) gene cause congenital chloride diarrhoea. Nat Genet 1996; 14(3): 316–319. [PubMed: 8896562]
43. Yang H, Jiang W, Furth EE, Wen X, Katz JP, Sellon RK et al. Intestinal inflammation reduces expression of DRA, a transporter responsible for congenital chloride diarrhea. Am J Physiol 1998; 275(6 Pt 1): G1445–1453. [PubMed: 9843783]
44. Lohi H, Makela S, Pulkkinen K, Hoglund P, Karjalainen-Lindsberg ML, Puolakkainen P et al. Upregulation of CFTR expression but not SLC26A3 and SLC9A3 in ulcerative colitis. Am J Physiol Gastrointest Liver Physiol 2002; 283(3): G567–575. [PubMed: 12181169]
45. Ding X, Li D, Li M, Wang H, He Q, Wang Y et al. SLC26A3 (DRA) prevents TNF-alpha-induced barrier dysfunction and dextran sulfate sodium-induced acute colitis. Lab Invest 2018; 98(4): 462–476. [PubMed: 29330471]
46. Jacob P, Rossmann H, Lamprecht G, Kretz A, Neff C, Lin-Wu E et al. Down-regulated in adenoma mediates apical Cl−/HCO3− exchange in rabbit, rat, and human duodenum. Gastroenterology 2002; 122(3): 709–724. [PubMed: 11875004]
47. Schweinfest CW, Spyropoulos DD, Henderson KW, Kim JH, Chapman JM, Barone S et al. slc26a3 (dra)-deficient mice display chloride-losing diarrhea, enhanced colonic proliferation, and distinct up-regulation of ion transporters in the colon. J Biol Chem 2006; 281(49): 37962–37971. [PubMed: 17001077]
48. Hayashi H, Suruga K, Yamashita Y. Regulation of intestinal Cl−/HCO3− exchanger SLC26A3 by intracellular pH. Am J Physiol Cell Physiol 2009; 296(6): C1279–1290. [PubMed: 19321737]
49. Ding X, Li D, Li M, Tian D, Yu H, Yu Q. Tumor necrosis factor-alpha acts reciprocally with solute carrier family 26, member 3, (downregulated-in-adenoma) and reduces its expression, leading to intestinal inflammation. Int J Mol Med 2018; 41(3): 1224–1232. [PubMed: 29286110]

50. Sartor RB. Current concepts of the etiology and pathogenesis of ulcerative colitis and Crohn's disease. Gastroenterol Clin North Am 1995; 24(3): 475–507. [PubMed: 8809232]
51. Sartor RB. Mechanisms of disease: pathogenesis of Crohn's disease and ulcerative colitis. Nat Clin Pract Gastroenterol Hepatol 2006; 3(7): 390–407. [PubMed: 16819502]
52. Thoreson R, Cullen JJ. Pathophysiology of inflammatory bowel disease: an overview. Surg Clin North Am 2007; 87(3): 575–585. [PubMed: 17560413]
53. Silveira ALM, Ferreira AVM, de Oliveira MC, Rachid MA, da Cunha Sousa LF, Dos Santos Martins F et al. Preventive rather than therapeutic treatment with high fiber diet attenuates clinical and inflammatory markers of acute and chronic DSS-induced colitis in mice. Eur J Nutr 2017; 56(1): 179–191. [PubMed: 26458966]
54. Farooq SM, Stadnyk AW. Neutrophil infiltration of the colon is independent of the FPR1 yet FPR1 deficient mice show differential susceptibilities to acute versus chronic induced colitis. Dig Dis Sci 2012; 57(7): 1802–1812. [PubMed: 22383080]
55. Eltzschig HK, Bratton DL, Colgan SP. Targeting hypoxia signalling for the treatment of ischaemic and inflammatory diseases. Nat Rev Drug Discov 2014; 13(11): 852–869.. [PubMed: 25359381]
56. Campbell EL, Louis NA, Tomassetti SE, Canny GO, Arita M, Serhan CN et al. Resolvin E1 promotes mucosal surface clearance of neutrophils: a new paradigm for inflammatory resolution. Faseb J 2007; 21(12): 3162–3170. [PubMed: 17496159]
57. Mahe MM, Aihara E, Schumacher MA, Zavros Y, Montrose MH, Helmrath MA et al. Establishment of Gastrointestinal Epithelial Organoids. Curr Protoc Mouse Biol 2013; 3(4): 217–240. [PubMed: 25105065]
58. Miyoshi H, Ajima R, Luo CT, Yamaguchi TP, Stappenbeck TS. Wnt5a potentiates TGF-beta signaling to promote colonic crypt regeneration after tissue injury. Science 2012; 338(6103): 108–113. [PubMed: 22956684]
59. Finkbeiner SR, Hill DR, Altheim CH, Dedhia PH, Taylor MJ, Tsai YH et al. Transcriptome-wide Analysis Reveals Hallmarks of Human Intestine Development and Maturation In Vitro and In Vivo. Stem Cell Reports 2015.
60. Jones JC, Brindley CD, Elder NH, Myers MG Jr., Rajala MW, Dekaney CM et al. Cellular Plasticity of Defa4(Cre)-Expressing Paneth Cells in Response to Notch Activation and Intestinal Injury. Celi Mol Gastroenterol Hepatol 2019; 7(3): 533–554.
61. Sanjana NE, Shalem O, Zhang F. Improved vectors and genome-wide libraries for CRISPR screening. Nat Methods 2014; 11(8): 783–784. [PubMed: 25075903]
62. Zhang L, Yang C, Chen S, Wang G, Shi B, Tao X et al. Long Noncoding RNA DANCR Is a Positive Regulator of Proliferation and Chondrogenic Differentiation in Human Synovium-Derived Stem Cells. DNA Cell Biol 2017; 36(2): 136–142. [PubMed: 27982693]
63. Weissmuller T, Campbell EL, Rosenberger P, Scully M, Beck PL, Furuta GT et al. PMNs facilitate translocation of platelets across human and mouse epithelium and together alter fluid homeostasis via epithelial cell-expressed ecto-NTPDases. J Clin Invest 2008; 118(11): 3682–3692. [PubMed: 18924612]
64. Madara JL, Patapoff TW, Gillece-Castro B, Colgan SP, Parkos CA, Delp C et al. 5'-adenosine monophosphate is the neutrophil-derived paracrine factor that elicits chloride secretion from T84 intestinal epithelial cell monolayers. J Clin Invest 1993; 91(5): 2320–2325. [PubMed: 8486793]
65. Grant RL, Acosta D. Ratiometric measurement of intracellular pH of cultured cells with BCECF in a fluorescence multi-well plate reader. In Vitro Cell Dev Biol Anim 1997; 33(4): 256–260. [PubMed: 9156340]
66. Hartley Z, Dubinsky JM. Changes in intracellular pH associated with glutamate excitotoxicity. J Neurosci 1993; 13(11): 4690–4699. [PubMed: 7901350]

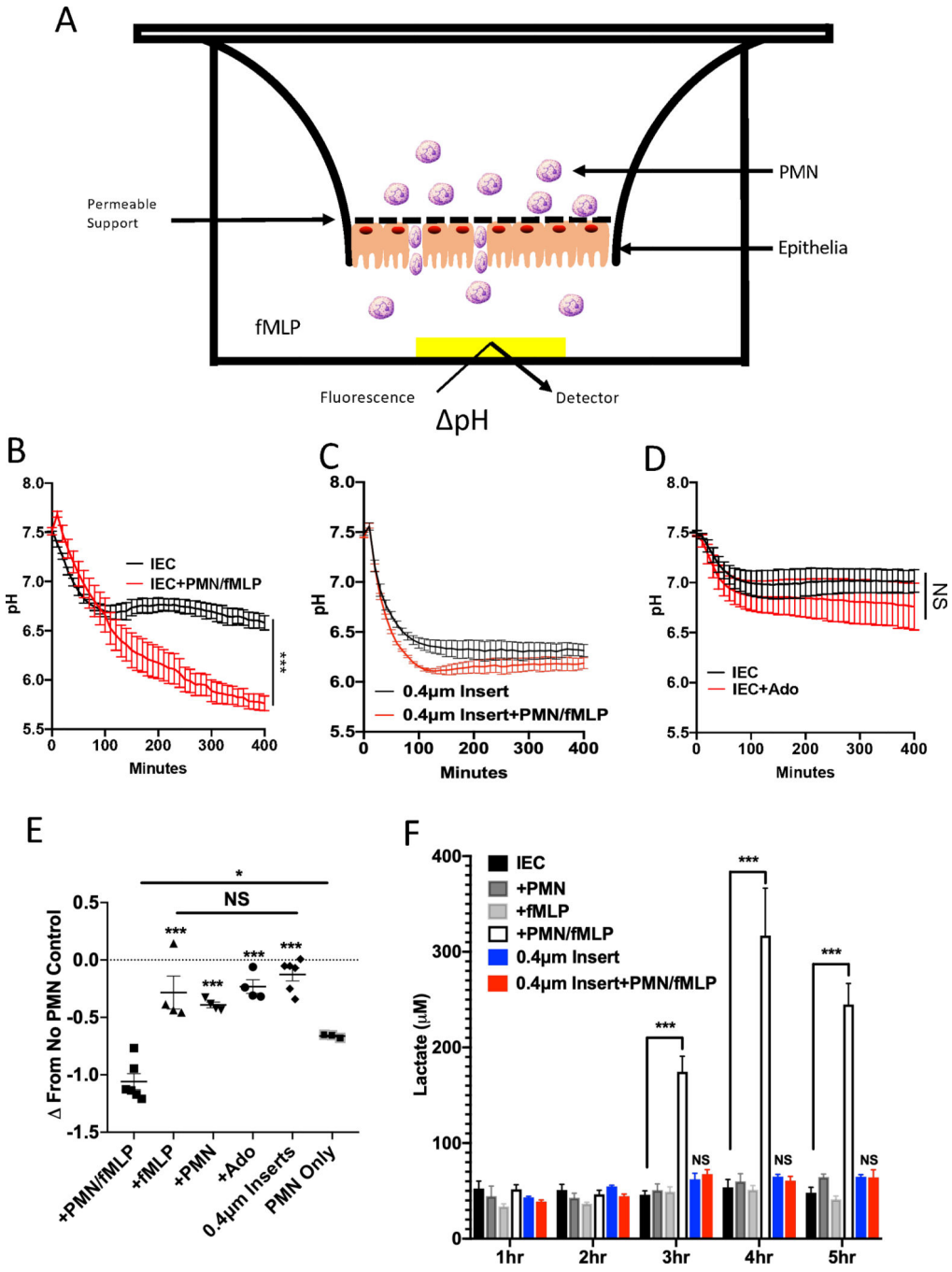

Figure 1: Influence of extracellular pH by PMN transmigration.

(A) Model of extracellular pH monitoring assay. (B-D) Changes in extracellular pH. 1×10^6 PMN were transmigrated across confluent T84 monolayers and the extracellular pH was recorded every minute for 400 min. Data are expressed as pH (n=3–6). (E) At T400 the difference in pH between controls and activated PMN treated monolayers were calculated. Data are expressed at change in pH. (F) Quantification of secreted lactate (n=3). n=number of independent experiments performed, separate passages of cells were used for each

experiment. The data for each experiment was pooled and expressed as the mean ± SEM and p-value determined by ANOVA or T-test. *p<0.01, **p<0.001, ***p<0.0001

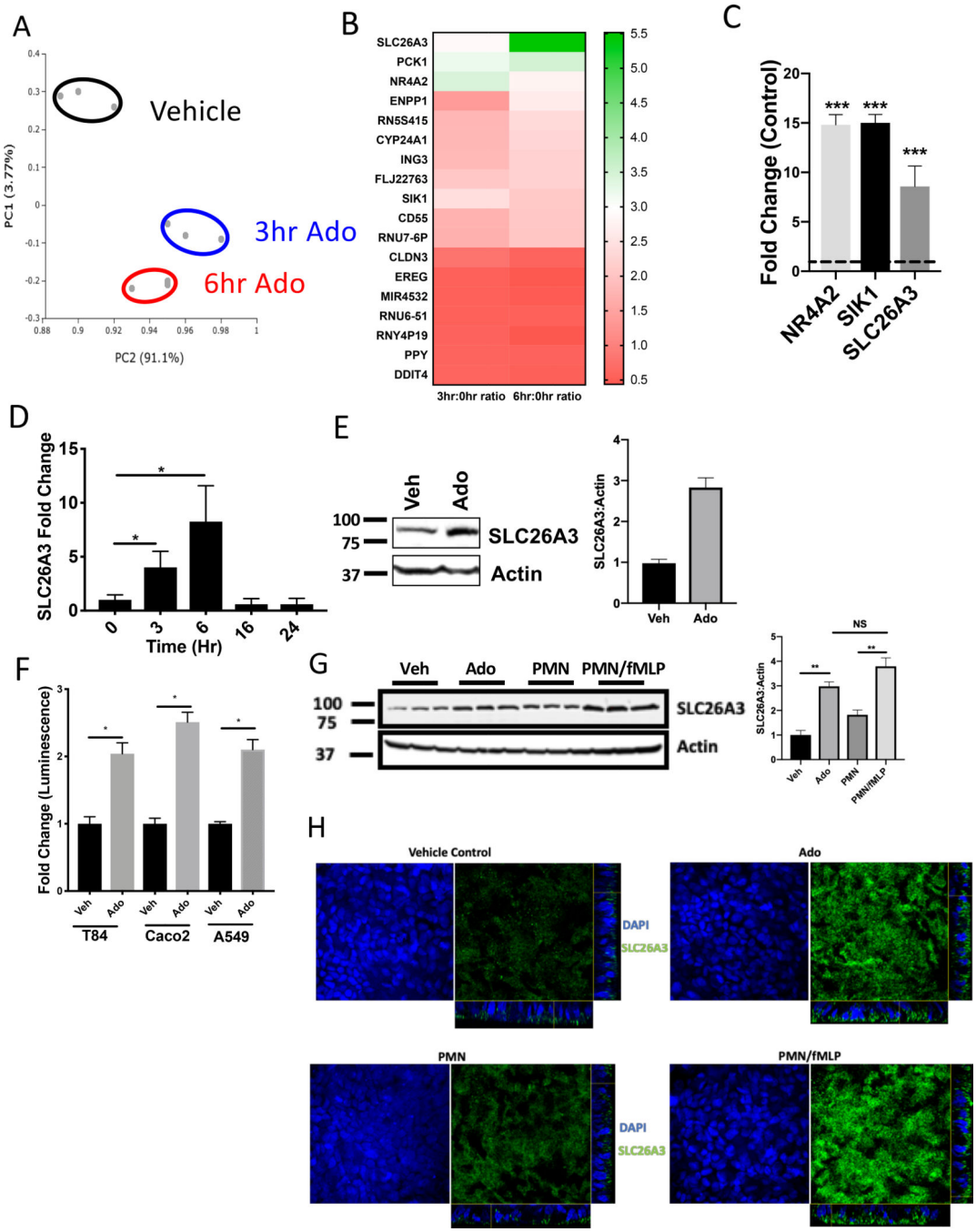

Figure 2: Microarray analysis of adenosine-treated intestinal epithelial cells.

(A) Principal component analysis (PCA) of the Ado microarray. (B) Top genes induced and repressed by 3 or 6 hr 100 μM Ado treatment (n=3). (C) Validation of induced expression of NR4A2, SIK1, and SLC26A3 by 6 hr 100 μM Ado treatment. Data expressed as Fold change compared to respective controls (n=3). (D) Time course of SLC26A3 transcript expression following treatment with 100 μM Ado (n=3). (E) Representative western blot and densitometry analysis of SLC26A3 expression following 24 hr 100 μM Ado treatment (n=3). (F) Luciferase promoter assay of induced expression of SLC26A3 in T84, Caco2, and A459

by 3 hr 100 μM Ado treatment (n=3). (G) Western blot and densitometry of SLC26A3 24 hr post PMN TEM (n=3). (H) Representative confocal images of DAPI and SLC26A3 expression in T84 IECs following PMN TEM. (B-F) n=number of independent experiments performed, separate passages of cells were used for each experiment. The data for each experiment was pooled and expressed as the mean ± SEM and p-value determined by T-test. * indicated $p< 0.01$, ** indicated $p<0.001$., *** indicates $p<0.0001$.

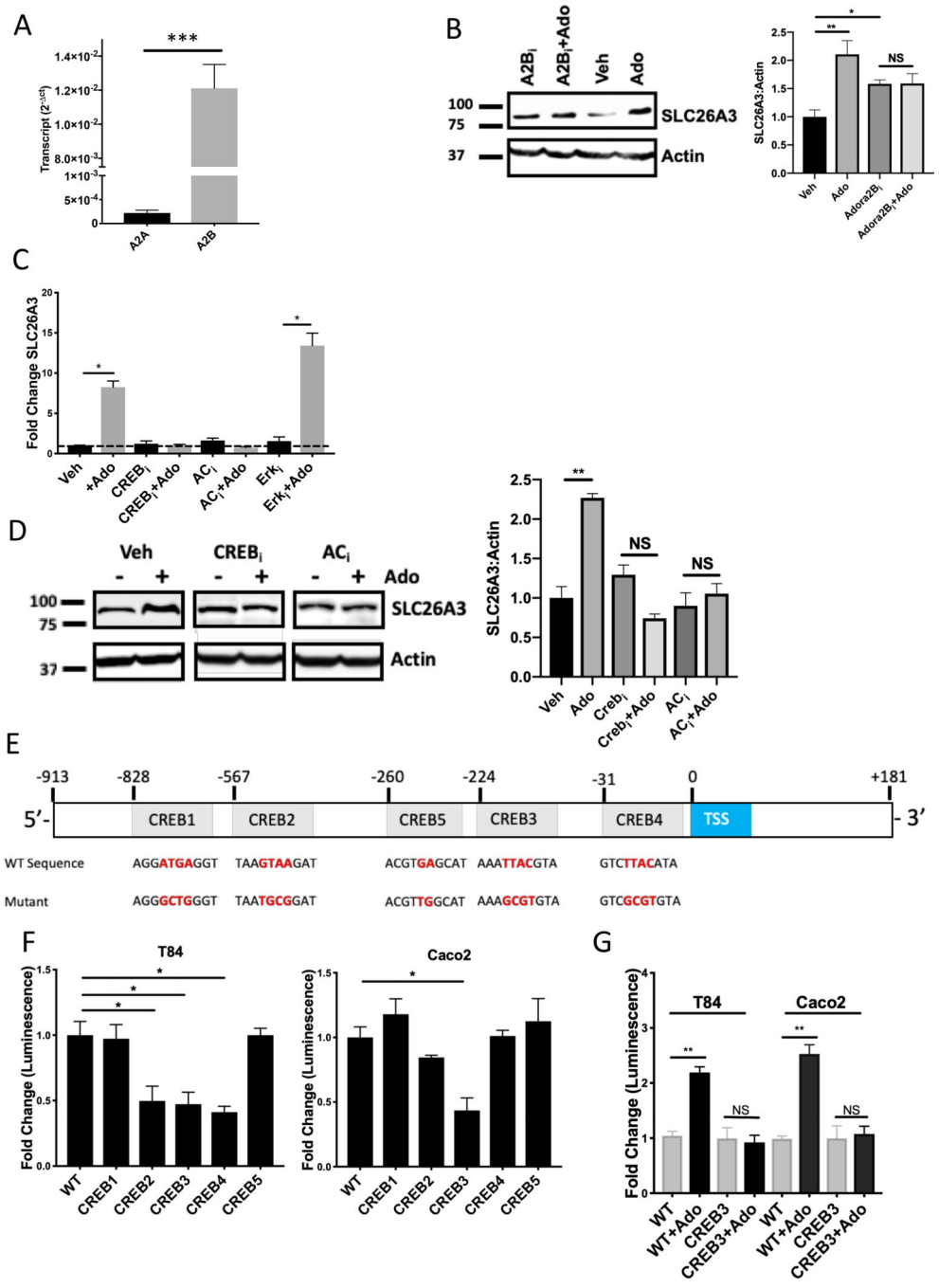

Figure 3: CREB/cAMP dependent expression of SLC26A3 by Ado.

(A) RT-PCR quantification of adenosine receptor A2A and A2B expression in T84 IECs (n=3). (B) Western blot analysis of SLC26A3 in T84 treated with 1 μM PSB603 ± 24 hr 100 μM Ado treatment (n=3). (C) Induced expression of SLC26A3 by 6 hr 100 μM Ado treatment in T84 IECs with a 1 hr pretreatment with either 30 μM Erk, 1 μM CREB, or 10μM adenylyl cyclase inhibitor via transcript (n=3). (D) Representative western blot and densitometry analysis of SLC26A3 expression at 24 hr following 100 μM Ado treatment in T84 IECs pretreated with 1μM CREB or 10 μM adenylyl cyclase inhibitors (n=3). (E)

SLC26A3 promoter map with WT and mutated CREB sites. (F&G) Analysis of baseline and 3 hr 100 μM Ado treatment SLC26A3 promoter activity in CREB mutants in both T84 and Caco2 IECs via luciferase promoter assay (n=3). n=number of independent experiments performed, separate passages of cells were used for each experiment. The data for each experiment was pooled and expressed as the mean ± SEM and p-value determined by T-test. * indicate $p< 0.01$, ** $p<0.001$, ***$p<0.0001$

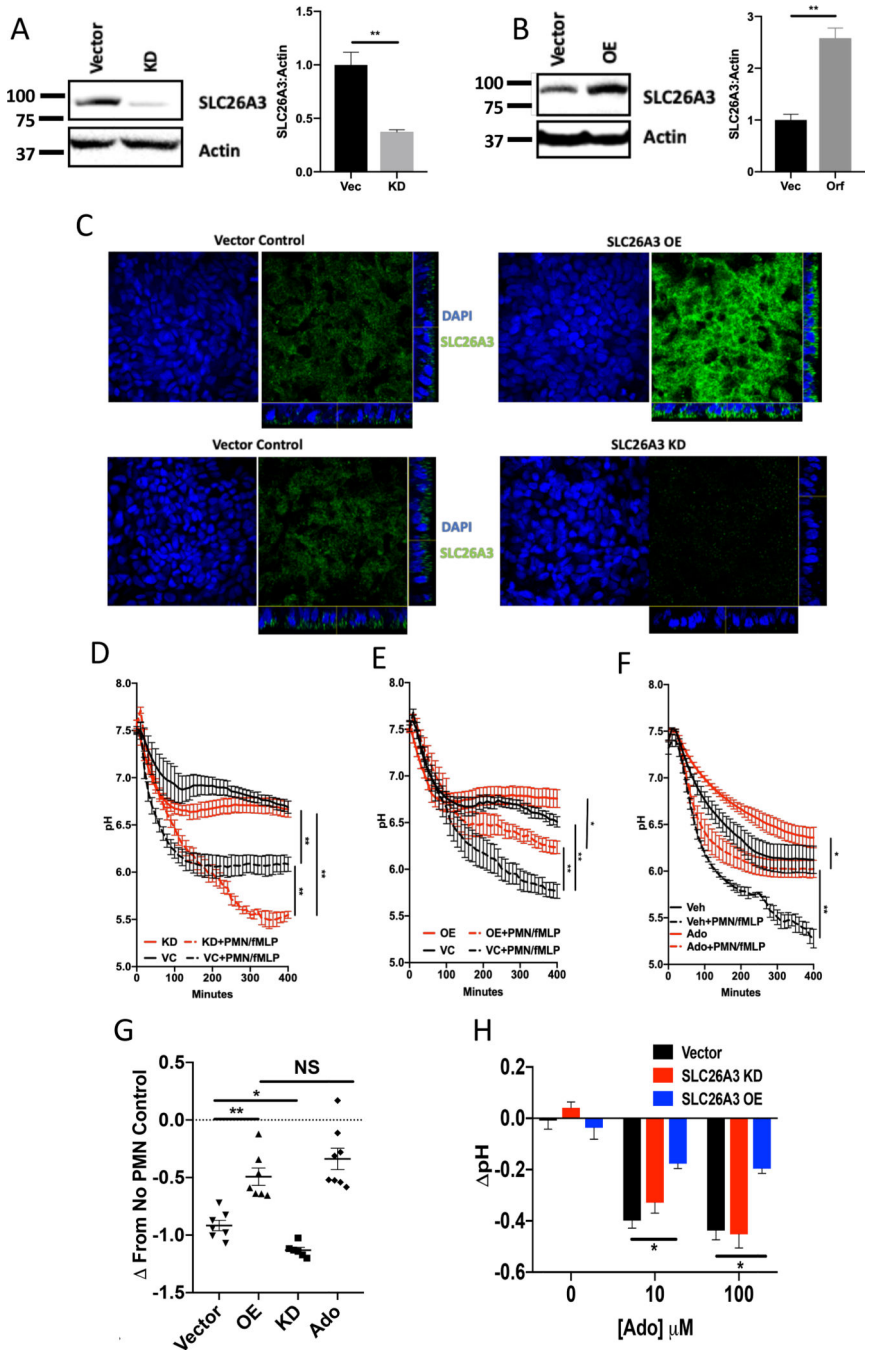

Figure 4: Impact of SLC26A3 on cellular homeostasis.

(A-B) Representative western blot and densitometry analysis of SLC26A3 expression in CRISPR-mediated lentiviral transduced cells or Orf-mediated lentiviral transduced cells (n=3). (C) Confocal images of SLC26A3 expression in vector controls, OE, and KD T84 IECs. Main image is a condensed z-stack and inserts depict the orthogonal view of the stacked image. (D-E) Analysis of extracellular pH following PMN transmigration over the course of 400 min in KD and OE T84 IECs (n=6–8). (F) Analysis of extracellular pH following PMN transmigration over the course of 400 min in T84 IECs pretreated with 100

μM Ado for 24 hr. (G) Change in pH between PMN exposed and non-PMN exposed IECs Vector, KD, OE, and 24hr Ado pretreated cells at T400. (H) Change in intracellular pH between T0 and T120 min in vector control, KD, and OE cells treated with 0, 10, or 100 μM Ado (n=3). n=number of independent experiments performed, separate passages of cells were used for each experiment. The data for each experiment was pooled and expressed as the mean ± SEM and p-value determined by ANOVA or T-test, * indicate $p< 0.01$, **$p<0.001$

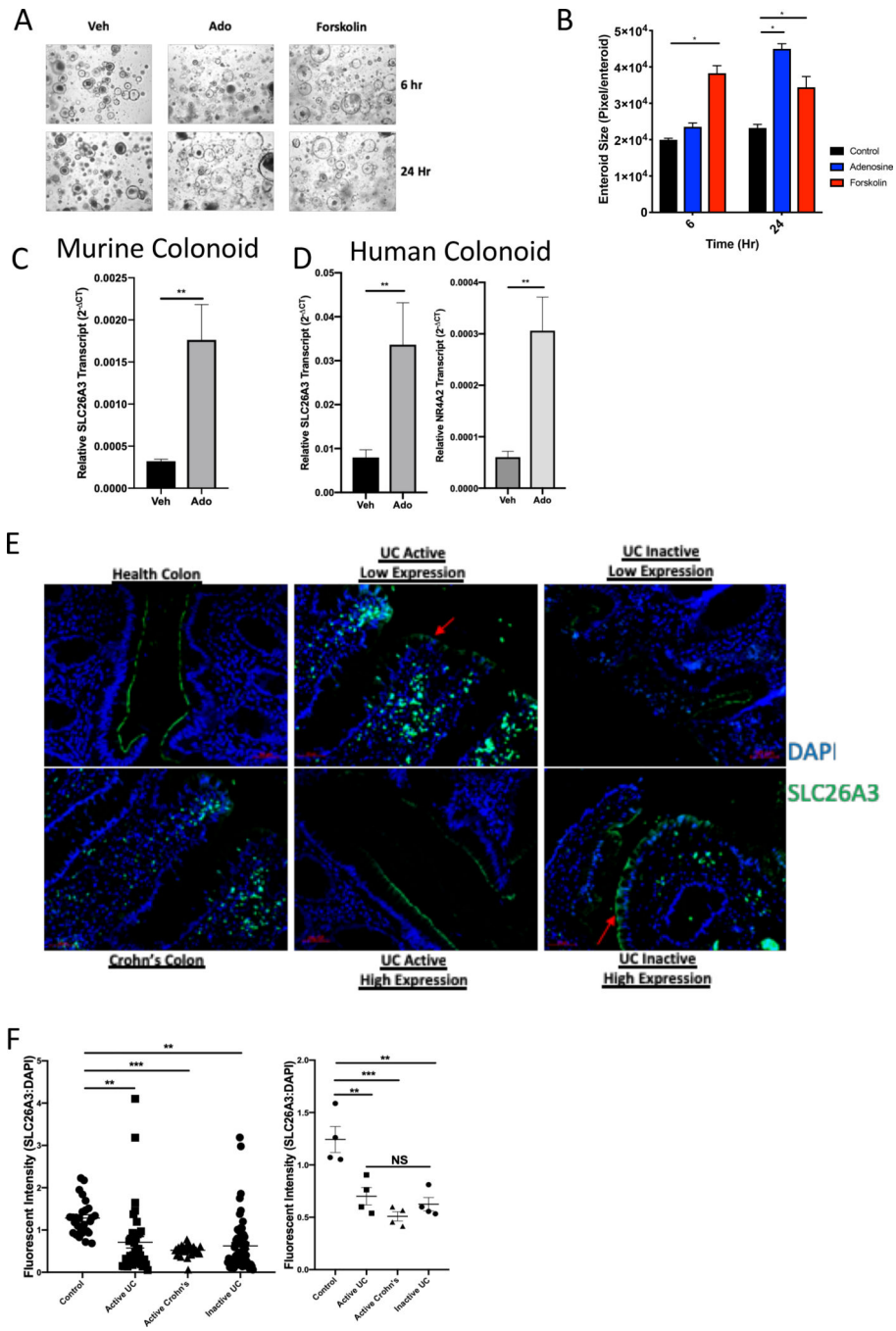

Figure 5: SLC26A3 expression in non-transformed cells and active disease.

(A) Brightfield images of respective colonoids following 6 and 24 hr 100 μM Ado or 10 μM forskolin treatment. (B) The size of C57BL/6 derived intestinal colonoidss treated with 100 μM Ado or 10 μM forskolin were quantified by measuring the pixels/colonoid at 6 and 24 hr (n=3). (C) Induced SLC26A3 expression by 3 hr 100 μM Ado treatment in mouse colonic colonoids via RT-PCR (n=3). (D) Induced SLC26A3 and NR4A2 expression by 3 hr 100 μM Ado treatment in human colonoids via RT-PCR (n=3). (E) Representative confocal images depicting localization and expression of SLC26A3 (Green) and DAPI (Blue) in control,

Crohn's, active UC, and inactive UC colons. (F) Quantification of epithelial specific SLC26A3 expression via fluorescent intensity ratio between SLC26A3 and DAPI in control, Crohn's, active UC, and inactive UC colons. Data expressed as both the average of each experiment (right) and individual valúes (left) (n=4). n=number of independent experiments performed, separate passages of cells were used for each experiment. The data for each experiment was pooled and expressed as the mean ± SEM and p-value determined by ANOVA or T-test, * $p < 0.01$, ** $p < 0.001$, ** $p < 0.0001$

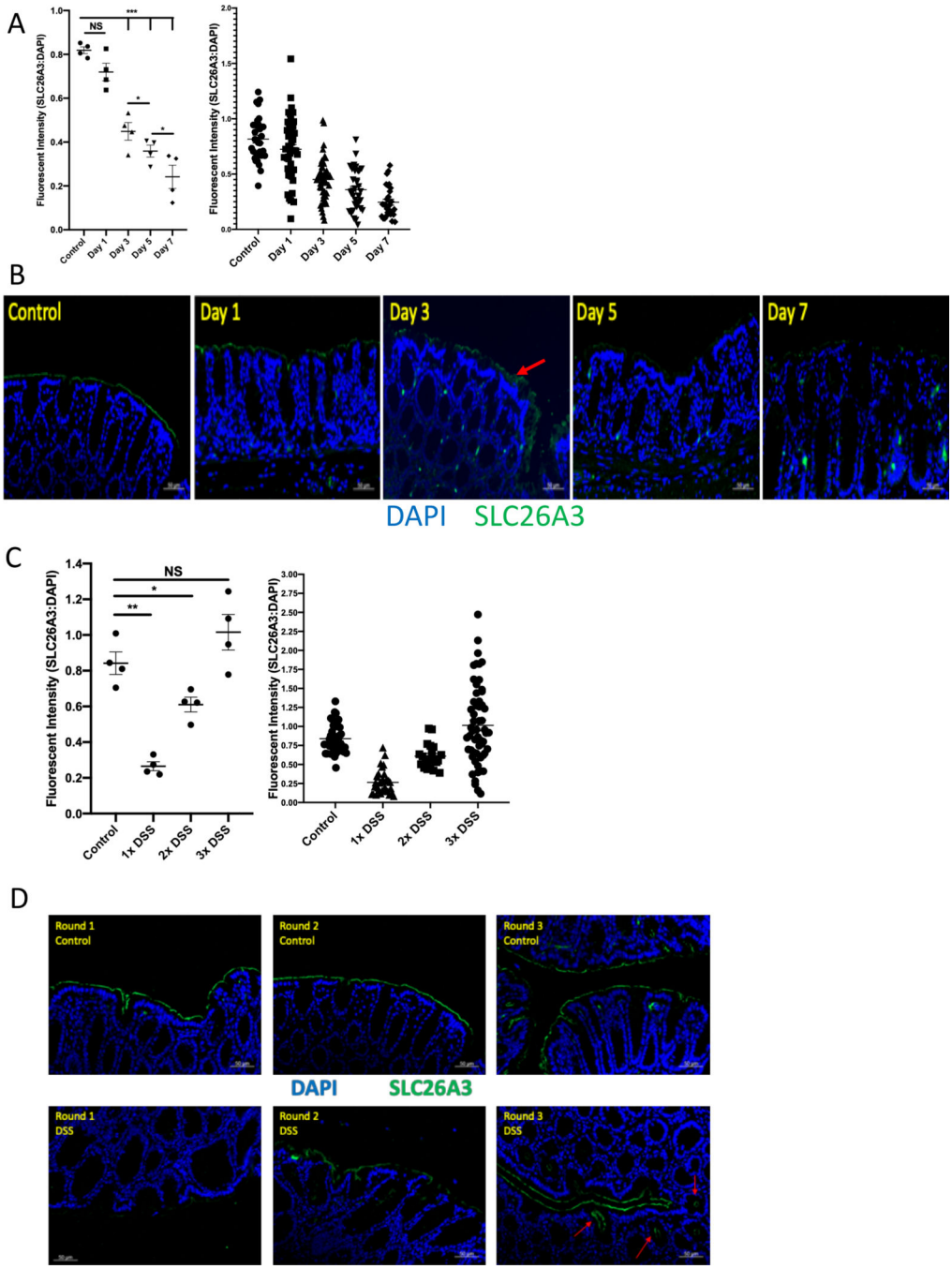

Figure 6: SLC26A3 expression in DSS induced colitis.

(A) Quantification of epithelial specific SLC26A3 expression via fluorescent intensity ratio between SLC26A3 and DAPI in control and DSS treated mice. Data expressed as both the average of each experiment (left) and individual values (right) (n=4). (B) Representative confocal images depicting localization and expression of SLC26A3 (Green) and DAPI (Blue) in mice treated with 3% DSS or H20 for 1, 3, 5, and 7 days. (C) Quantification of epithelial specific SLC26A3 expression via fluorescent intensity ratio between SLC26A3 and DAPI in control and chronic DSS treated mice. Data expressed as both the average of

each experiment (left) and individual values (right) (n=4). (D) Representative confocal images depicting localization and expression of SLC26A3 (Green) and DAPI (Blue) in control mice and mice treated with 1, 2, or 3 rounds of 3% DSS. n=number of independent experiments performed, separate passages of cells were used for each experiment. The data for each experiment was pooled and expressed as the mean ± SEM and p-value determined by ANOVA or T-test, * $p < 0.01$, ** $p < 0.001$, *** $p < 0.0001$

Table 1

Predicted pH verse Observed pH

	1 Hr	2 Hr	3 Hr	4 Hr	5 Hr
Control Predicted	7.22±0.0U	7.23±0.009	7.23±0.006	7.22±0.12	7.23±0.0078
Control Observed	6.83±0.044	6.69±0.076	6.75±0.077	6.75±0.068	6.70±0.074
Mean Difference	0.40±0.043 p<0.0001	0.54±0.076 p<0.0001	0.48±0.077 p<0.0001	0.47±0.068 p<0.0001	0.53±0.074 p<0.0001
+PMN Predicted	7.23±0.0077	7.23±0.0059	6.97±0.019	6.72±0.11	6.89±0.060
+PMN Observed	6.98±0.14	6.46±0.15	6.21±0.17	6.07±0.15	5.89±0.11
Mean Difference	0.26±0.16 p=0.42	0.78±0.19 p=0.0006	0.76±0.16 p<0.0001	0.65±0.15 p=0.0003	1.00±0.16 p<0.0001

Table 2

Real-Time PCR Primers

Gene Target	Forward Primer	Reverse Primer
SLC26A3 (Human)	5′-CGGAGGCGAGACTACCACA-3′	5′- ACC A A A ACCG GGAGGTGTTG-3′
SLC26A3 (Mouse)	5′-GCCGTGGTTGGGAACATGA-3′	5 ′ -G C A A ATCCTTTG A ATG CTCC AG -3′
NR4A2 (Human)	5 ′-GTTCAG G CG CAGTATG GGTC-3′	5′-CTCCCGAAGAGTG GTAACTGT-3′
NR4A3 (Human)	5′-CATACAG CT CG G A ATACACCAC-3′	5′-CCCTCCACGAAGGTACTGATG-3′
SIK1 (Human)	5′ -CT CCG G GTG G GTTTTTACG AC-3′	5′-CTGCGTTTTGGTGACTCGATG-3′
β -actin (Human)	5′ -G C ACT CTT CCAG CCTT CCTT CC-3′	5′-CAGGTCTTTGCGGATGTCCACG-3′
β-actin (Mouse)	5 ′-AACCCTAAG G CCAACCGTG AA-3′	5 ′-T C ACG CACG ATTT CCCT CTCA-3 ′
ADORA2A (Human)	5′ -CG CTCCG GTACA ATG G CTT-3′	5′-TTGTTCCAACCTAGCATGGGA-3′
ADORA2B (Human)	5′-TGCACTGACTTCTACGGCTG-3′	5′-GGTCCCCGTGACCAAACTT-3′
cFOS (Human)	5′-GGGGCAAGGTGGAACAGTTAT-3′	5′-CCGCTTGGAGTGTATCAGTCA-3′